JOURNAL OF Applied Polymer SCIENCE

Structure and Property Changes of Polyamide 6 During the Gel-Spinning Process

Huimin Zhang,[1] Chaoming Shi,[1] Miaomiao He,[2] Qingxiu Jia,[1] Liqun Zhang[2]

[1]Beijing Key Laboratory of Clothing Materials R&D and Assessment, Beijing Institute of Fashion Technology, Beijing 100029, China

[2]Key Laboratory of Beijing City for the Preparation and Processing of Novel Polymer Materials, Beijing University of Chemical Technology, Beijing 100029, China

Correspondence to: Q. Jia (E-mail: jiaqingxiu@163.com) or L. Zhang (E-mail: zhanglq@mail.buct.edu.cn)

ABSTRACT: Polyamide 6 (PA6) gels were prepared by the dissolution of PA6 powder in formic acid with $CaCl_2$ as a complexing agent. The concentration of the polymer was 16% w/v. PA6 fibers were obtained through gel-spinning, drawing, decomplexation, and heat-setting processes. The structure and properties of the fibers at different stages were characterized with differential scanning calorimetry, thermogravimetric analysis, X-ray diffraction, Fourier transform infrared spectroscopy, and scanning electron microscopy. The experiment results indicate that the melting transition of the as-spun fibers obtained by the extrusion of the PA6/$CaCl_2$/HCOOH solution into a coagulation bath through a die disappeared. A porous structure existed in the as-spun fibers, which led to poor mechanical properties. Compared with the as-spun fibers, the melting and glass-transition temperatures of the decomplexed and drawn fibers retained their original values from PA6, the degree of crystallinity increased, the porous structure disappeared, and the mechanical properties were improved. The maximum modulus and tensile strength obtained from the drawn fibers in this study were 32.3 GPa and 530.5 MPa, respectively, at the maximum draw ratio of 10. © 2013 Wiley Periodicals, Inc. J. Appl. Polym. Sci. 130: 4449–4456, 2013

KEYWORDS: fibers; polyamides; structure–property relations

Received 19 December 2012; accepted 14 May 2013; Published online 24 July 2013

DOI: 10.1002/app.39542

INTRODUCTION

Polyamide 6 (PA6) is more prone to crystallization, wear, and dyeing, with its planar zigzag and flexible chain structure, compared to polyethylene and poly(vinyl alcohol). The theoretical modulus of PA6 fibers is 263 GPa,[1] and the theoretical tensile strength is up to one-tenth that of the elastic modulus; this shows promise for PA6 fibers to be high-performance fibers. However, with normal processing techniques, the elastic modulus of PA6 fiber is only 4–5 GPa[2] because the maximum draw ratio is approximately 5, which is much lower than the draw ratio of polyethylene. The hydrogen bonds between polyamide molecules in the amorphous and crystal domains restrict the achievement of a high draw ratio and a high molecular orientation; this leads to a failure to achieve a high-strength and high-modulus nylon fiber.

The key to preparing high-performance PA6 fibers is to suppress hydrogen bonding between molecular chains to overcome the low maximum draw ratio. For this reason, appropriate complexing agents are needed to temporarily suppress hydrogen bonding during drawing and improve the maximum draw ratio. At the same time, the hydrogen bonds reform easily, and this allows the molecular interactions to be strengthened after the drawing process. Iodine, anhydrous NH_3, and metal chlorides are commonly used complexing agents at present. Lee and Porter[3] found that there was considerable chain slippage in nylon 6 during the stretching process when iodine was used as a plasticizer, and the complexed nylon 6 showed an initial modulus of only 3 GPa. Zachariades and Porter[4] reported the reversible plasticization of PA6 and polyamide 11 through the addition of anhydrous NH_3. Acierno et al.[5] found that the orientation of PA6 could be improved with lithium chloride, and this resulted in an increase in the modulus of the fibers.

Wu et al.[6] adopted $GaCl_3$ for the complexation of high-relative-viscosity PA6 and found that the complexing membrane system could be stretched 20 times, however, with serious slippage between molecules. The molecular orientation did not improve significantly, and this limited the fiber performance improvement. In our previous study,[7] a detailed comparison of the complexation of several complexing agents for PA6 was made, and we found that calcium chloride had a stronger complexing ability. The coordination mechanism between calcium chloride

and PA6 amide were characterized with IR spectroscopy and X-ray photoelectron spectroscopy.[8] PA6 fibers with a modulus of up to 70.4 GPa could be prepared by gel spinning.[9]

The key factor for the fabrication of high-strength and high-modulus fibers from such nonrigid polymers is how to extend and orient the folded polymer chains along the fiber axis to a very high degree. So, the key technology of the gel spinning is the quenching of the as-spun fibers in a cryogenic coagulation bath to maintain the macromolecular disentanglement state. In addition, to improve the uniformity of the fibers, the concentration of the coagulation bath must generally be high to suppress the double diffusion between the as-spun fibers and the coagulation bath. Thus, as-spun fibers with fewer entanglement points are obtained, which are prone to ultradrawing. Thereby, the difference between general dry-jet wet spinning and gel spinning is the different state of the as-spun fibers in the coagulation bath rather than the spinning process.

Gel spinning is a commonly used technique for preparing high-strength and high-modulus fibers, and it has been successfully used in the production of high-performance fibers.[10–13] It is important to explore the mechanism of gel spinning and the preparation of high-performance fibers through the investigation of the structure and properties of fibers at different stages in the gel spinning process.[14–18] In our previous study, PA6 fibers with a maximum draw ratio of 8 and an initial modulus of 28.8 GPa were first obtained by the gel spinning process. A proper coagulation and optimum parameters of the gel spinning process for the PA6/calcium chloride/formic acid system were selected. In this study, we studied the changes in the structure and properties of fibers in the gel spinning of a PA6/$CaCl_2$/formic acid system in detail. The evolution of the thermal properties, functional group structure, crystallization properties, degree of orientation, microstructure, and mechanical properties of PA6 macromolecules in the gel spinning process was investigated. The results obtained give a better interpretation of the spinning process, which will be helpful in the development of the gel spinning method and to prepare PA6 fibers with a higher strength and higher modulus.

EXPERIMENTAL

Materials

Ultrahigh-molecular-weight PA6 with a relative viscosity of 18.46 was prepared by the slurry anionic polymerization of caprolactam with sodium hydroxide as a catalyst, diisocyanate as an activator, and inert aliphatic hydrocarbon as the dispersant. The polymerization was carried out *in vacuo* at pressures in the range 20–30 Pa and at temperatures in the range 140–150°C. The viscosity of the samples was measured by an Ostwald viscometer. After polymerization, the PA6 powder was dried at 70°C in a vacuum oven for 24 h before complexation. Formic acid (98 wt %), chloroform, and anhydrous $CaCl_2$ were analytical grade and were used as received.

Preparation of the PA6 Complex Solutions and Gel Spinning

The PA6/$CaCl_2$/HCOOH spinning solutions were prepared by the dissolution of PA6 powder in formic acid with $CaCl_2$ as a complexing agent under nitrogen at room temperature. The concentration of PA6 was 16 wt %, and the molar ratio of $CaCl_2$ to PA6 repeating units was 0.15. Mechanical stirring was used to dissolve the polymer completely, and then, centrifugation was carried out for 15 min to remove air bubbles. PA6/HCOOH solutions were prepared in a similar manner.

A miniature spinning apparatus was used for gel spinning. Fibers were extruded at a temperature of 40°C through a die with a diameter of 0.5 mm and a length of 5 mm. The as-spun fibers were quenched to 8°C in 0.50–0.65-m coagulation bath composed of 50 vol % tetrachloroethane and 50 vol % dichloromethane and then placed in a 0.10–0.12-m air spinning tunnel to form the complexed original fibers (COFs). The COFs were collected on bobbins at a low speed of 3–4 cm/s and dried under ambient conditions.

The drawing of the gel fibers was carried out by a two-stage draw process. In the first stage of drawing, the fibers were stretched to certain multiples of their original length at ambient temperature. Then, the fibers were immersed in a mixture of 50 vol % ethanol and 50 vol % water in a beaker for 4 h to form the uncomplexed fiber (UF). In the next step, the second stage of drawing was carried out at 175°C to various draw ratios. Then, the finished fibers (FFs) were formed after 1–2 min at a heat setting of 175°C.

Characterization and Tests

Differential scanning calorimetry (DSC) analysis was performed on a Seiko DSC 6200 instrument (Japan) under a nitrogen atmosphere at a flow rate of 50 mL/min. The measurement of all samples consisted of three consecutive scans: (1) heating from room temperature to 250°C at a scanning rate of 50°C/min and keeping the temperature at 250°C for 5 min to remove the heat history, (2) cooling from 250 to 25°C at a scanning rate of 10°C/min to get the curve of cooling, and (3) heating from 25 to 250°C at a scanning rate of 10°C/min to get the curve of heating. Al_2O_3 was taken as the reference sample. The melting temperatures (T_m's) of the samples were taken as the maximum of the melting peaks in the heating curves, and the T_g values were taken at the midpoint of glass-transition in the heating curves.

The measurement of wide-angle X-ray scattering was carried out with a Rigaku X-ray diffractometer (Japan) with curved-crystal monochromatized Cu Kα radiation (1.54 Å) generated at 40 kV and 50 mA. Equatorial scans were obtained in the 2θ range of 6–36° with intensity data collected. The crystallinity (X_c), crystal forms, and crystal size of the sample were calculated with the device X-ray diffraction (XRD) processing software.

Fourier transform infrared (FTIR) spectra were obtained from attenuated total reflectance on a Nicolet nexus 670 spectrometer (Thermo Co.). At least 64 scans were obtained at attenuated total reflectance to achieve an adequate signal-to-noise ratio.

The morphology of the fibers was observed with a field emission scanning electron microscope (JSM-6360SEM, Japan). The cross sections of the fiber samples were prepared by cutting the samples at room temperature, and they were sputter-coated with gold.

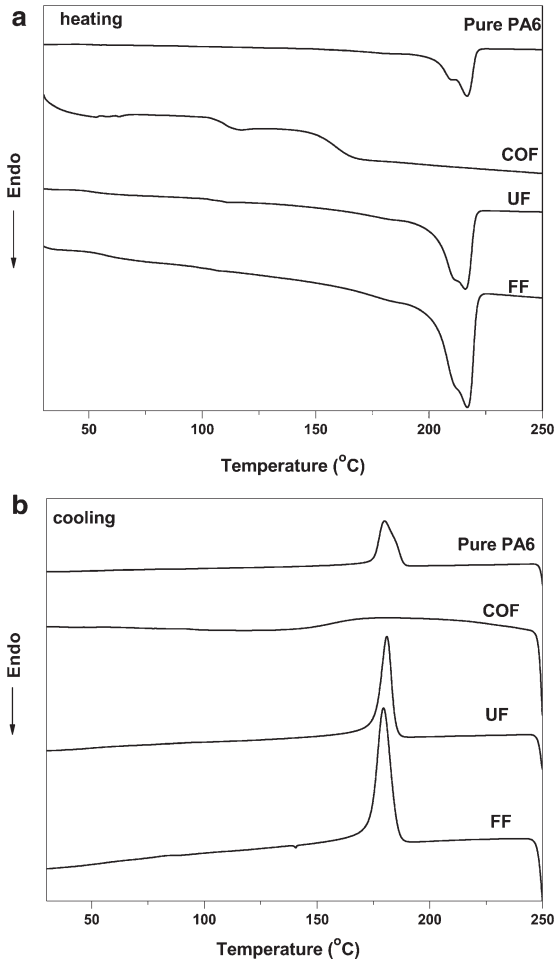

Figure 1. DSC scans of the pure PA6 and fiber samples at different stages observed upon (a) heating and (b) cooling.

The tensile properties of the fibers were measured with a YG-004N single-fiber electronic strength tester at a clamping length of 10 mm and a tensile speed of 40 mm/min. The test conditions were kept at 25 ± 2°C and 35 ± 3% relative humidity. Ten specimens were tested for each sample.

The thermal decomposition properties were tested on a Mettler-Toledo TGA/DSC1 STARe system instrument (Switzerland) under a nitrogen atmosphere and at a scanning rate of 20°C/min.

The birefringence (Δn) was measured by a BX41-P polarizing microscope equipped with a Senarmont compensator. A sodium lamp was used as a light source.

Table I. DSC Parameters of the Pure PA6 and Different Fiber Samples at Different Stages

Sample	T_{g1} (°C)	T_{g2} (°C)	T_{g3} (°C)	T_m (°C)	T_{cc} (°C)
Pure PA6	48.5	—	—	216.6	180.0
COF	50.3	109.0	157.9	—	—
UF	51.7	—	—	216.0	180.9
FF	54.4	—	—	216.9	179.4

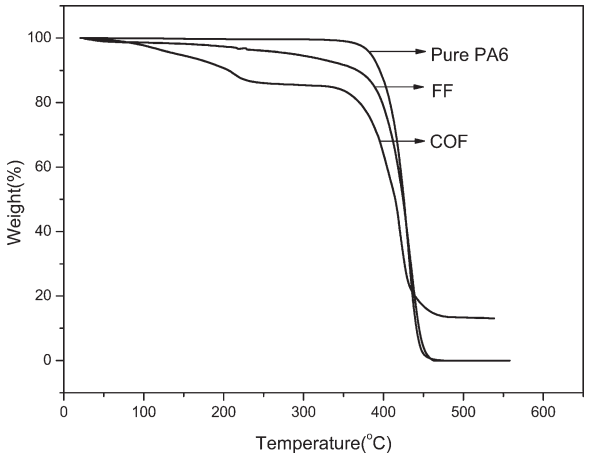

Figure 2. TG scans of the COF and FF samples.

RESULTS AND DISCUSSION

Thermal Analysis

Figure 1 gives the DSC results obtained for the pure PA6 powder, COF, UF, and FF upon heating. The T_m, glass-transition temperature (T_g), and crystallization temperature (T_{cc}) of all of the samples are shown in Table I. The DSC scans of all of the samples displayed glass transitions (T_{g1}'s) as described in the literature,[19,20] which were related to the stretching movement temperature of the unoriented parts in the amorphous domain. Compared with the pure PA6 powder, COF had two more T_g's (T_{g2} and T_{g3}), which were attributed to the decrease in the molecular hydrogen bonds from the complexation between the $CaCl_2$ and PA6 molecules. This glass transition happened in a higher temperature range because of the complexation, which limited movement of the molecular chains. After decomplexation, the UF displays only T_{g1} at 51.7°C; this indicated that hydrogen bonds re-formed. After drawing, T_{g1} of the FF shifted to a higher temperature because of the orientation of the amorphous phase.

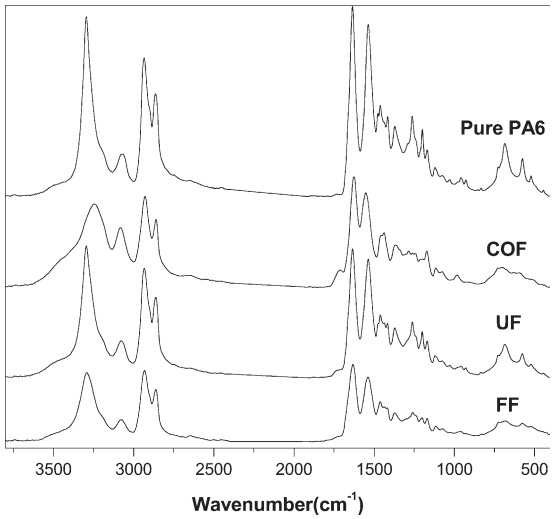

Figure 3. FTIR spectra of the pure PA6 and fiber samples at different stages.

Table II. Data from the IR Absorption Spectra for the Main Groups of the Pure PA6 and Different Fiber Samples at Different Stages

Sample	υ_{N-H}	$\upsilon_{C=O}$	υ_{C-N}	υ_{sCH2}	υ_{asCH2}
Pure PA6	3294.5	1634.9	1537.2	2863.8	2934.4
COF	3245.7	1625.7	1553.0	2859.8	2928.8
UF	3294.7	1634.6	1537.3	2862.1	2933.5
FF	3292.6	1632.6	1538.2	2861.6	2932.2

The DSC scan of the pure PA6 sample displayed obvious double melting peaks at 216°C. Crystallization was reflected directly during the melting process. During crystallization, as the temperature decreased, the melt viscosity increased rapidly, and the mobility of the molecular chain decreased; this caused misorientation of the crystallite regions. The less perfect crystals (γ polymorphs) melted at lower temperatures, and the more perfect crystals (α crystal form) melted at higher temperatures; this resulted in a wide melting range.[21] The double melting behavior was also found in UF and FF and indicated that the drawing and heat-setting processes had no significant influence on that.

The thermal analysis curve of the COF displayed no melting peak in the DSC heating process at a constant rate. Because the number and density of the hydrogen bonds decreased after the $CaCl_2$ shielded the hydrogen bonds between the amide linkages in PA6, the crystallization of PA6 was hindered, and the melting process of PA6 was promoted. After decomplexation, $CaCl_2$ was removed, and the hydrogen bonds were restored; this enhanced the forces between the molecular chains and resulted in an increase in T_m. T_m of the fibers further increased after stretching and heat setting and reached the T_m of pure PA6, which was attributed to the orientation-induced crystallization of the FFs.

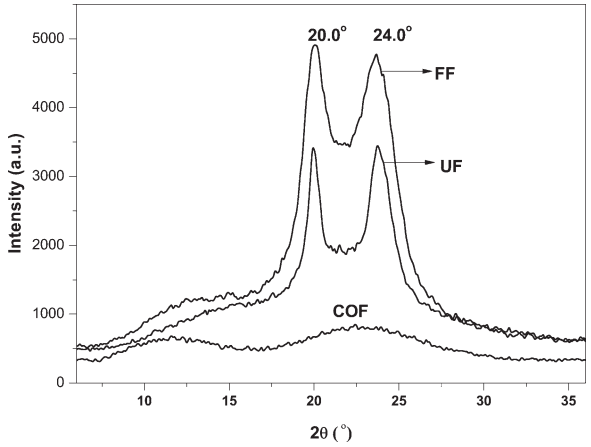

Figure 4. XRD spectra of the fiber samples at different stages.

The structural change in PA6 after complexation was further confirmed by the cooling cycle of DSC analysis. As shown in Figure 1, during the cooling process, the crystallization of the complexed PA6 was hindered by the addition of $CaCl_2$ because the complex compound formed between the $CaCl_2$ and PA6 molecular chains replaced the hydrogen bonds between the molecular chains and restricted the molecular chain movement. Thus, it was difficult to form a crystal structure, the size of the crystals decreased, the distance between them increased, and the integrity of the crystals was poor. The crystallization rate and crystallinity of PA6 decreased, and this resulted in an amorphous structure. The COF displayed no crystalline peaks in the cooling curve; this indicated that the PA6 crystallinity and crystallization rate could be effectively controlled by the addition of $CaCl_2$. After the removal of $CaCl_2$, the hydrogen-bond interaction between the PA6 molecular chains recovered, and the crystallinity increased; this resulted in the crystallization of UF and FF close the T_{cc} of pure PA6.

Thermogravimetric (TG) Analysis

Figure 2 shows the TG curves of the samples at different stages. As shown in Figure 2, the TG curve of FF and pure PA6 coincided generally, and there was only one big mass loss step; this decomposition began at 370°C and was complete at 480°C. On the other hand, COF slowly lost mass from room temperature to 240°C, and this was attributed to the residual formic acid. Then, the weight decreased rapidly at about 360°C, and unlike pure PA6, the curve became flat at about 480°C, but the weight was not reduced to zero. The residue no longer decomposed in the test range; this residue was calcium in the COF system. Figure 2 shows that there were no $CaCl_2$ residues in the FF; this indicated that the decomplexation was thoroughly completed.

FTIR Spectroscopy Analysis

Infrared spectroscopy is an important testing tool for testing molecular structure and interactions; it is very effective for characterizing the interaction between the complexing agent and polyamide. In the polyamide 66/LiCl[20] system, the formation of a six-membered ring strengthened hydrogen-bond interactions and caused the N—H vibration bond (υ_{N-H}) to shift to a lower frequency and the C=O vibration bond ($\upsilon_{C=O}$) in the amide I band to shift to a higher frequency. On the other hand, in the polyamide 66/$GaCl_3$[21] system, the carbonyl group of PA6 formed a coordination complex with $GaCl_3$, and the N—H bond was free; this caused the N—H vibration bond (υ_{N-H}) to

Table III. Crystallinity and Crystal Shape Changes of the Different Fiber Samples at Different Stages

Sample	X_c (%)	γ Crystallinity (%)	α Crystallinity (%)	γ Grain size (Å)	α-1 Grain size (Å)	α-2 Grain size (Å)
COF	—	—	—	—	—	—
UF	47.5	7.1	92.9	52.8	114.0	59.9
FF	61.3	9.5	90.5	77.9	60.9	41.1

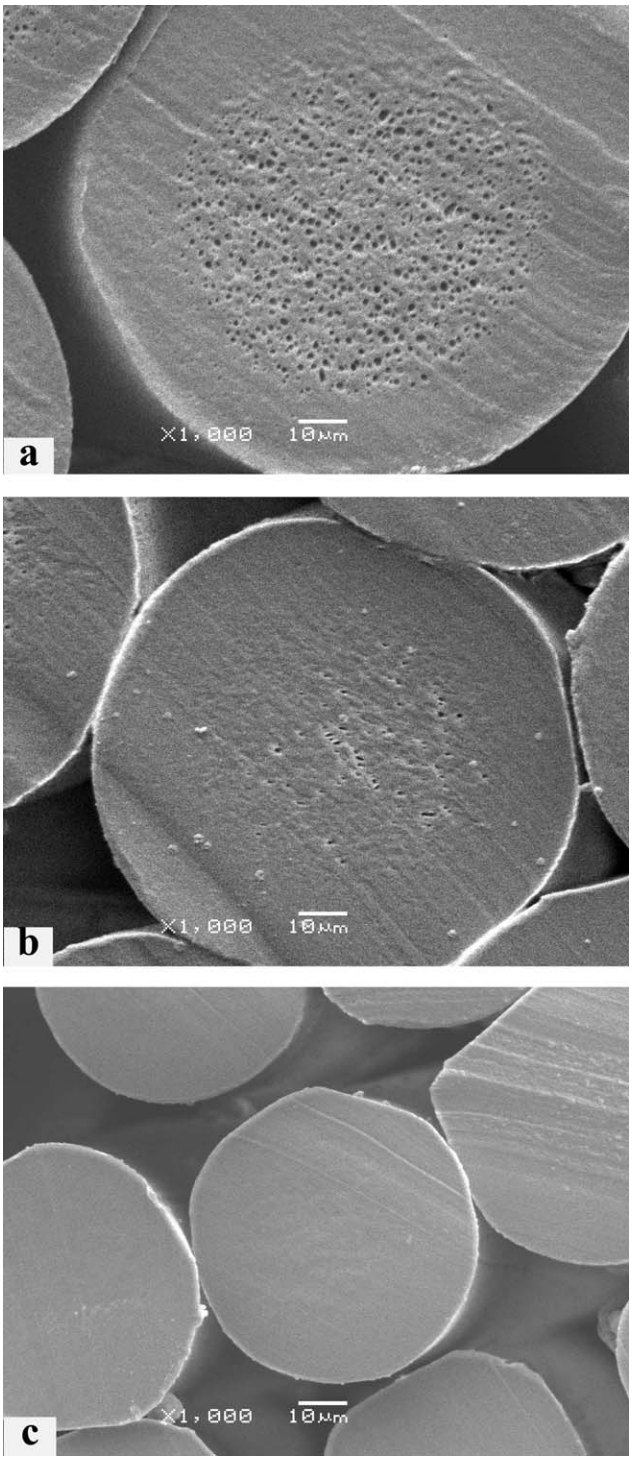

Figure 5. SEM micrographs of the cross sections of (a) COF, (b) UF, and (c) FF.

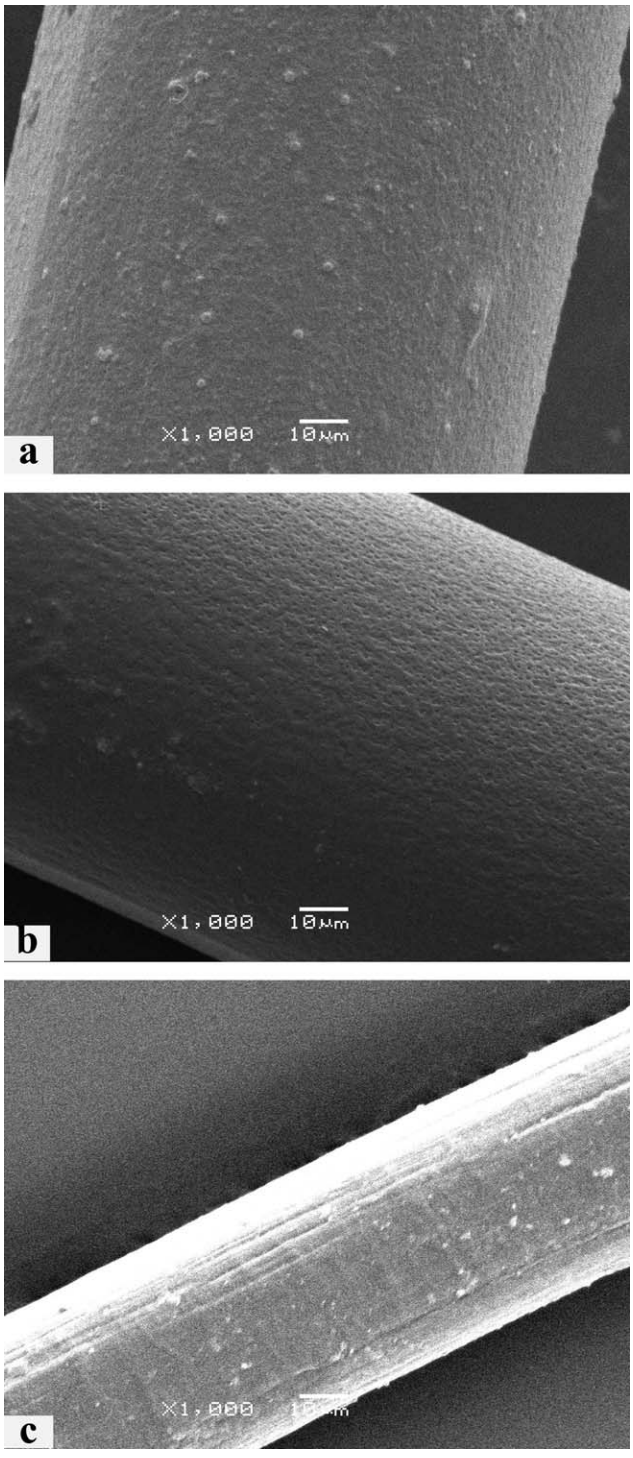

Figure 6. SEM of micrograph of the surfaces of (a) COF, (b) UF, and (c) FF.

shift to a higher frequency and the C═O vibration bond ($\upsilon_{C=O}$) to shift to a lower frequency.

Figure 3 shows the FTIR spectra of the pure PA6 and fiber samples at different stages. The data of the IR absorption spectra for the main groups of all of the samples are summarized in Table II. Compared with pure PA6, the C═O band of COF shifted to a lower frequency, from 1634.9 to 1625.7 cm^{-1}; this was similar to previous findings.[8] In COF, the carbonyl group of PA6 formed a coordination complex with $CaCl_2$. Because the coordination complex formed by calcium ions and carbonyl groups was more stable compared with the hydrogen bonds formed between the PA6 chains, the vibration motion of the carbonyl group became more difficult because of the stronger

Table IV. Degree of Orientation of the Different Fiber Samples at Different Stages

Sample	Interference fringe	Offset angle (°)	Diameter (μm)	Δn (10^{-3})
COF	0	0	69	—
UF	3	95	51	40.7
	3	93	56	37.0
	3	89	59	34.9
FF	4	93	40	45.1
	5	89	45	49.8
	5	88	48	49.7

induction effect of the positive charge in the calcium ion.[22] After decomplexation for 4 h, $CaCl_2$ was removed, and the hydrogen bonds were recovered, so the IR spectrum of UF was very similar to that of pure PA6; this was consistent with the DSC results. Compared with UF, the N—H vibration bond (υ_{N-H}) and C=O vibration bond ($\upsilon_{C=O}$) of FF shifted to a slightly lower frequency because the density and interaction of hydrogen bonds between the PA6 chains increased because of stretching.

XRD Analysis

Nylon 6 has a variety of crystal structures, of which the α- and γ-crystalline phases are the most common.[23–26] The former has hydrogen bonds between antiparallel chains, and the latter has hydrogen bonds between parallel chains, with half the number of intermolecular hydrogen bonds as the former. It can be seen from the diffraction curves of the various crystalline variants that the α-crystalline phase consists predominantly of two characteristic diffraction peaks of (200) and (002) (reflections at 20.2 and 23.9°, respectively), whereas the γ-crystalline phase consists predominantly of one characteristic diffraction peak of (200) (shoulders at 21.3°). When the two variants coexist, the three peaks will overlap.[23,24]

Figure 4 shows the XRD patterns of the various fiber samples at different spinning stages, and the X_c, crystal type, and crystal size of each sample are given in Table III. COF displayed no obvious crystalline form; this indicated that hydrogen-bond interactions were weakened and PA6 crystallization behavior was hindered by the addition of $CaCl_2$. This reduced the relative viscosity, improved the processing performance, and allowed the fiber to be stretched at a high draw ratio. After complete decomplexation treatment of UF, $CaCl_2$ was removed, and the hydrogen bonds were recovered. So the molecular chains had sufficient time to move and form a stable crystalline structure. Compared with UF, FF also consisted of α- and γ-crystalline phases with similar proportions. However, the degrees of crystallinity of FF and UF were 61.3 and 47.5%, respectively; these values were attributed to the process of drawing to 10 times the fibers' original length at room temperature, decomplexation, and heat setting. The high ratio drawing increased the degree of fiber orientation and led to a more orderly arrangement of macromolecular chains. In addition, the hydrogen bonds between molecular chains recovered after decomplexation and resulted in stronger molecular interactions and a higher crystallinity. The crystal size decreased for the α-crystalline phase and increased for the γ-crystalline phase of FF. However, the content of the α-crystalline phase was much larger than the crystalline phase; this was also attributed to the more orderly and compact arrangement of PA6 molecular chains after high-ratio drawing.

Scanning Electron Microscopy (SEM)

Figure 5 shows the SEM micrographs of the cross sections of the fibers at different stages. As shown in Figure 5, the cross section of the fiber was in round shape; this indicated good fiber formation after the tetrachloroethane–methylene chloride cosolvent coagulation bath at a low temperature of 8°C. COF appeared to have an obvious skin–core structure and a lot of hollow bubbles or porous structures inside the fibers; the reason was that in the tensile zone of the spinneret, when the cortex solidified, the core was still in the flow state, so that the spinning tension focused on the surface of the gel layer to cause a uniaxial tensile deformation, orientation of the macromolecules, and chain segments along the fiber axis, and only a very small part of the tension resulted in a uniaxial elongational flow of the core. This produced different degrees of orientation along the fiber layers; in addition, after the orientation of drawing, the macromolecular chains of the outer layer in the spinneret holes quickly froze in the coagulation bath. However, the rate of solidification was slow for the inner layer, so disorientation of the orientation part of the molecular chain might have also contributed to the skin–core structure. The formation of hollow bubbles or porous structures was due to double diffusion of the solvent and coagulant in the spinning process; this resulted in the phase separation of the formic acid and spinning solution. A cortex formed on the surface of the fibers at first, and then, the formic acid diffused through the cortex, and methylene chloride and tetrachloroethane penetrated from the coagulation bath. This caused a change in the spinning liquid volume and the solidification inside. Because there existed some solvent inside the fibers after solidification, after the solvent was evaporated, pores formed in the spun fibers. When necessary, these pores could be removed by a drying densification process.

After the stretching, decomplexation, and heat treatment, calcium chloride was removed. Because of the recovery of hydrogen bonds, the arrangement between the molecular chains became denser, the hollow bubbles or porous structures in the UF decreased, and the diameter of the fiber was smaller than

Table V. Mechanical Performance of the Different Fiber Samples at Different Stages

Sample	Draw ratio	Tensile strength (MPa)	Initial modulus (GPa)	Ultimate elongation (%)
COF	1	54.2	0.2	398.2
UF	1	71.8	0.5	381.6
FF	10	530.5	32.3	27.1

that of COF. In addition to the decomplexation and heat setting, FF was prepared through a 10-fold drawing processing; this resulted in a more compact arrangement of PA6 molecular chains. Therefore, the pores disappeared in the cross section of the fiber, and the fiber diameter was further reduced.

Figure 6 shows SEM photographs of the surface of the fibers at different stages. Excessive $CaCl_2$ was found on the surface of COF. After the calcium chloride was removed, very fine microholes were produced on the surface of UF. A microfibrillated structure formed after high-ratio drawing, and this resulted in a significant vertical orientation structure. The small amount of $CaCl_2$ residue was also found on the surface of UF and FF, but it had little effect on the fiber properties.

Orientation

The orientation of fibers refers to the arrangement of molecular chains or other structural units along the external force direction. The oriented structure had an extremely important influence on the mechanical properties of fiber. After the degree of orientation was increased, the breaking strength of the fibers improved. After orientation, the molecular chains arranged in a more orderly manner, and the system entropy decreased. Therefore, inherently, the structure tended to change from an ordered to a disordered state. To obtain high-strength fibers, usually, the fibers need to be stretched at a high draw ratio, during which the polymer will also crystallize.

Fiber orientation was obtained by the measurement of Δn with an optical microscope. Table IV shows the degree of orientation of the fiber samples at different stages; these data indicate that COF had no orientation without the appearance of interference fringes and further confirmed that there was no crystallization in COF because of hydrogen-bond being shielded. The fiber orientation was improved after decomplexation and stretch processing.

Mechanical Properties

Table V shows the mechanical properties of the fiber samples at different spinning stages. Factors affecting the mechanical properties of the PA6 fibers included the relative viscosity of the PA6 raw material, spinning condition, decomplexation condition, and the drawing and heat setting processes. The decomplexation and drawing processing were the main factors in this study. As shown in Table IV, the mechanical properties of the fiber changed significantly after decomplexation. After decomplexation, the breaking strength and initial modulus of the fibers increased. Because the hydrogen bonds were shielded in COF, the degree of crystallinity and strength of the fibers were low. After decomplexation for 4 h, the hydrogen bonds recovered, and the degree of crystallinity increased; this resulted in the improvement of the mechanical properties. After the drawing, decomplexation, and heat setting processes, the breaking strength and initial modulus of FF reached 530.5 MPa and 32.3 GPa, respectively. This was attributed to the increase in the crystallinity and degree of orientation after high-ratio drawing; this was consistent with the previous testing results of DSC and XRD.

CONCLUSIONS

PA6 fibers were obtained by the dissolution of PA6 powder in formic acid with $CaCl_2$ as a complexing agent through gel spinning, drawing, decomplexation, and heat-setting processes. The changes in the PA6 structure and properties in the spinning process were analyzed and are discussed in detail. The results show an amorphous and porous structure existed in COF, with the hydrogen bonds shielded with calcium chloride. After decomplexation, the fibers were semicrystalline, and calcium chloride was removed. The T_g and T_m values of FF were similar to those of pure PA6, and the mechanical properties were significantly higher than those of COF, with a much less porous structure in the fibers. The degree of orientation and crystallinity of FF further improved after high-ratio drawing and decomplexation processing. The maximum modulus and tensile strength obtained for the drawn fibers in this study were 32.3 and 530.5 GPa, respectively.

ACKNOWLEDGMENTS

Financial assistance was provided by the National Natural Science Foundation of China (grant 51273005), the Beijing Municipal Natural Science Foundation (grant 2092012), the New Star Plan of Science and Technology of Beijing (grant 2008B06), and the Beijing Natural Science Foundation Program and Scientific Research Key Program of the Beijing Municipal Commission of Education (grant KZ201110012016).

REFERENCES

1. Manley, D. R.; Martin, C. G. *Polymer* **1973**, *14*, 632.
2. Roberts, M. F.; Jenekhe, S. A. *Macromolecules* **1991**, *24*, 3142.
3. Lee, Y. H.; Porter, R. S. *J. Macromol. Sci. Phys.* **1995**, *34*, 295.
4. Zachariades, A. E.; Porter, R. S. *J. Appl. Polym. Sci.* **1979**, *24*, 1371.
5. Acierno, D.; La Mantia, F. P.; Ciferri, A.; Polizzotti, G. *J. Polym. Sci. Polym. Phys. Ed.* **1979**, *17*, 1903.
6. Wu, X. L.; Li, X. N.; Yang, Z. K.; Niu, Y. F.; Zhao, Y. X. *J. Beijing Inst. Clothing Technol.* **2006**, *26*, 1.
7. Jia, Q. X.; Xiong, Z. J.; Shi, C. M.; Zhang, L. Q.; Wang, X. N. *J. Appl. Polym. Sci.* **2012**, *124*, 5165.
8. Xiong, Z. J.; Li, X. N.; Jia, Q. X.; Fu, Z. Y.; Yang, Z. K. *Acta Polym. Sin.* **2010**, *8*, *1003*.
9. Jia, Q. X.; Xiong, Z. J.; Yang, Z. K.; Li, X. N.; Liu, Z. D.; Fu, Z. Y. Chin. Pat. 200910092063.3 (**2009**).
10. Smith, P.; Lemstra, P. *J. Colloid Polym. Sci.* **1980**, *258*, 891.
11. Godo, S.; Yasuo, O.; Syoji, O.; Tooru, K. U.S. Pat. 2005238875 A1 (**2005**).
12. Chae, H. G.; Minus, M. L.; Rasheeda, A.; Kumar, S. *Polymer* **2007**, *48*, 3781.
13. Yamaura, K.; Kumakura, M. *J. Appl. Polym. Sci.* **2000**, *77*, 2872.
14. Hoogsteen, W.; Hooft, R. J.; Postema, A. R.; Brinke, G.; Penning, A. J. *J. Mater. Sci.* **1988**, *23*, 3459.
15. Zhao, Y.; Yang, D. C. *Acta Polym. Sin.* **1994**, *6*, 647.
16. Xiao, C. F.; An, S. L.; Jia, G. X.; Zhang, Y. F. *Acta Polym. Sin.* **1999**, *2*, 171.

17. Vasanthan, N.; Kotek, R.; Jung, D. W.; Shin, D.; Tonelli, A. E.; Salem, D. R. *Polymer* **2004**, *45*, 4077.

18. Xu, N. K.; Xiao, C. F.; Song, Z. *Acta Polym. Sin.* **2009**, *1*, 317.

19. Khanna, Y. P.; Kuhn, W. P.; Sichina, W. *J. Macromolecules* **1995**, *28*, 2644.

20. Murthy, N. S. *J. Polym. Sci. Part B: Polym. Phys.* **2006**, *44*, 1763.

21. Yang, Z. K.; Yin, H. H.; Li, X. N.; Liu, Z. D.; Jia, Q. X. *J. Appl. Polym. Sci.* **2010**, *118* 1996.

22. Wu, J.; Xu, Y.; Zhang, J.; Zhao, Y.; Wang, S. F.; Xu, D. F.; Wu, J. G. *J. Appl. Polym. Sci.* **2004**, *91*, 2869.

23. Jung, D. W.; Kotek, R.; Vasanthan, N.; Tonelli, A. E. *Polym. Mater. Sci. Eng.* **2004**, *91*, 354.

24. Sun, B. H. *Chin. J. Polym. Sci.* **1994**, *12*, 57.

25. Holmes, D. R.; Bunn, C. W.; Smith, D. J. *J. Polym. Sci.* **1955**, *17*, 159.

26. Vogelsong. D. C. *J. Polym. Sci. Part A: Gen. Pap.* **1963**, *1*, 1055.